We are IntechOpen, the world's leading publisher of Open Access books Built by scientists, for scientists

4,800
Open access books available

122,000
International authors and editors

135M
Downloads

Our authors are among the

154
Countries delivered to

TOP 1%
most cited scientists

12.2%
Contributors from top 500 universities

CLARIVATE ANALYTICS BOOK CITATION INDEX INDEXED

WEB OF SCIENCE™

Selection of our books indexed in the Book Citation Index in Web of Science™ Core Collection (BKCI)

Interested in publishing with us?
Contact book.department@intechopen.com

Numbers displayed above are based on latest data collected.
For more information visit www.intechopen.com

6

New In-Situ Characterization Technique of Active Materials in Batteries: Electrochemical Acoustic Emission Method

Hiroshi Inoue
Osaka Prefecture University
Japan

1. Introduction

Active materials, reversible reactants at the positive and negative electrodes, in secondary batteries like lithium ion batteries and nickel-metalhydride (Ni-MH) batteries etc. expand and shrink their volume in charging and discharging processes. For example, in Ni-MH batteries, hydrogen storage alloy negative electrodes initially form hydrogen atoms (H_{ad}) on the alloy surface during the charging process (eq. 1).

$$H_2O + e^- \text{ --> } H_{ad} + OH^- \quad (1)$$

The resultant hydrogen atoms are absorbed into the alloy particles (eq. 2) while in the final stage of the charging process hydrogen evolution also occurs on the alloy surface (eq. 3).

$$H_{ad} \text{ --> } H_{ab} \quad (2)$$

$$2H_{ad} \text{ --> } H_2 \quad (3)$$

Here, H_{ab} is a hydrogen atom absorbed into alloy particles. When hydrogen atoms are absorbed into the alloy particles, their lattice volume expands. When the alloys absorb hydrogen atoms more and more, they eventually crack due to excessive strain. Consequently, fresh alloy surfaces appear, leading to improvement in reactivity for hydrogen absorption and discharge capacity, but the progress of the cracking causes the degradation of the alloys, leading to the decrease in discharge capacity. Therefore, characterization of the cracking, i.e. when and how the alloys crack, is important for the design of new alloys with higher performance. However, thus far, cracking of the alloys during charging has only been confirmed *ex situ* from scanning electron microscopy of the alloy surface.

Some *in situ* characterization techniques for the change in lattice volume of hydrogen storage alloys in charging have been developed. For example, *in situ* X-ray and neutron diffractometry clarified the relationship between lattice volume and state of charge, and phase transformation during charging in detail. On the other hand, i*n situ* scanning tunneling microscopy demonstrated reversible volume expansion of the secondary phase in a V-Ti-Ni-based multiphase alloy. However, these techniques are so skilled to get satisfactory data that simpler *in situ* techniques are desirable.

The acoustic emission (AE) method is a nondestructive and sensitive technique for detecting elastic waves generated by the cracking of materials. In addition, the AE method is a real time *in situ* analytical technique, and it's a low-priced method compared to X-ray and neutron diffractometry and STM. Physical phenomena such as corrosion, oxide formation, gas evolution, thin film rupture, cracking etc. can be discriminated by the AE method. In this chapter, I would like to introduce some examples in which the AE method was applied to the direct analysis of physical phenomena linked to electrochemical processes occurring at some hydrogen storage alloy negative electrodes during charging, including cracking of alloy particles and hydrogen evolution.

2. Experimental details

Ingots of $MmNi_{3.6}Mn_{0.4}Al_{0.3}Co_{0.7}$ (Mm: Mischmetal) and $TiCr_{0.3}V_{1.8}Ni_{0.3}$ alloys were prepared by an arc melting method in an Ar atmosphere. The mischmetal is a mixture of rare earth elements (La, Ce, Pr, Nd etc.). Each alloy ingot was ground into powder, and sieved into powders with particle sizes of 106-125 μm and less than 25 μm for the $MmNi_{3.6}Mn_{0.4}Al_{0.3}Co_{0.7}$ alloy and 75-106 μm and 25-53 μm for the $TiCr_{0.3}V_{1.8}Ni_{0.3}$ alloy. Each alloy powder was mixed with Cu powder with a mass ratio of 1:3, and the mixture was subjected to a pressure of 200 MPa at room temperature for 1 min to yield pellets for a negative electrode.

A typical experimental cell assembly for AE monitoring is shown in Fig. 1. The pellet-type negative electrode, a sulfonated-polypropylene separator and a $Ni(OH)_2/NiOOH$ positive electrode were stacked as shown in Fig. 1. A nickel sheet was used as a current collector for the negative electrode and protected the AE sensor from a 6M KOH aqueous solution which was used as the electrolyte. Before fabricating the cell assembly, the separator was thoroughly soaked in a 6M KOH aqueous solution. An Hg/HgO electrode was used as the reference electrode.

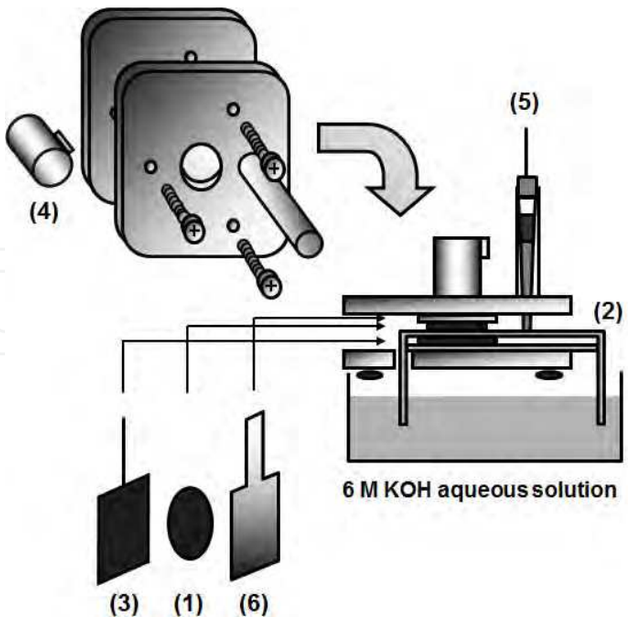

Fig. 1. A typical experimental cell assembly for monitoring AE signals. (1) Negative electrode, (2) Separator, (3) Positive electrode, (4) AE sensor, (5) Reference electrode, (6) Ni current collector.

The $MmNi_{3.6}Mn_{0.4}Al_{0.3}Co_{0.7}$ electrodes were charged at 100 mA g(alloy)$^{-1}$ for 3 h and discharged at 50 mA g(alloy)$^{-1}$ to -0.65 V vs. Hg/HgO, while the $TiV_{1.8}Cr_{0.3}Ni_{0.3}$ electrodes were charged at 100 mA g(alloy)$^{-1}$ for 6 h and discharged at 50 mA g(alloy)$^{-1}$ to -0.75 V vs. Hg/HgO. The unit "g(alloy)" means mass of alloy. After every charging the circuit was opened for 10 min. A setup for AE monitoring is shown in Fig. 2. An automatic AE monitoring system (NF Electronic Instruments, 7600/0710) was used for AE monitoring with an AE transducer (NF electronic Instruments, AE-900S-WB) and a preamplifier (30 dB gain for $MmNi_{3.6}Mn_{0.4}Al_{0.3}Co_{0.7}$ and 40 dB gain for $TiV_{1.8}Cr_{0.3}Ni_{0.3}$). The elastic waves generated by various phenomena such as cracking were detected by the AE transducer and transformed into AE signals. The AE signals were amplified by the preamplifier and stored in the automatic AE monitoring system. The stored data were displayed as time histories, power spectra and AE waveforms of the AE signals. The power spectra and AE waveforms express the distribution of frequencies for the AE signals and duration of the AE signals, respectively. All experiments were carried out at room temperature.

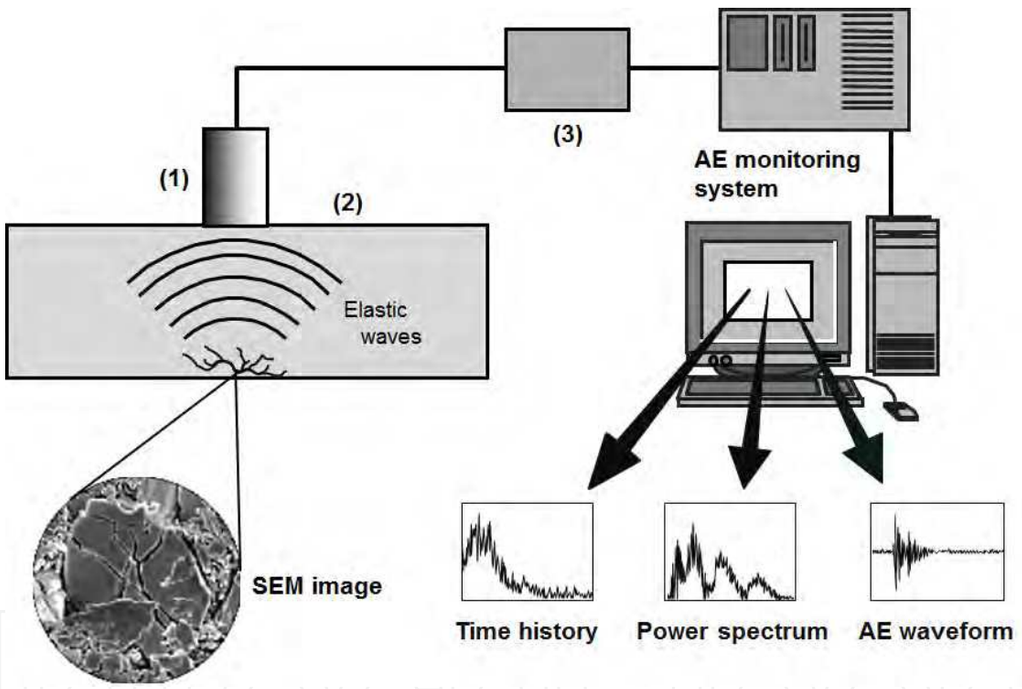

Fig. 2. A setup for AE monitoring. (1) AE transducer, (2) Sample, (3) Preamplifier.

3. Acoustic emission for hydrogen evolution on a copper electrode

During charging, hydrogen evolution occurs on the surface of the hydrogen storage alloy negative electrodes as a side reaction of the hydrogen absorption into the alloy. Not only the cracking of alloy particles but also the release of hydrogen bubbles on the electrode surface can be detected as AE signals. Figure 3 shows typical AE waveforms and power spectra for hydrogen evolution on a Cu electrode at -1.0 and -1.1 V vs. Hg/HgO. The AE waveforms at both applied potentials had long durations of over 0.15 ms. The AE waveform at –1.1 V had a larger maximum amplitude and longer duration than that at -1.0 V, suggesting hydrogen evolution at -1.1 V was more vigorous. As for power spectra, both had a relatively narrow frequency distribution of approximately 0.6 MHz and maximum amplitude at about 0.1

MHz. The AE waveforms and power spectra in Fig. 3 did not change with time. Sawai et al. have also obtained an AE waveform and power spectrum for hydrogen evolution when a sodium hydrogencarbonate aqueous solution was neutralized by dilute sulfuric acid. The present data for electrochemical hydrogen evolution were quite similar to their data. Therefore, the electrochemical hydrogen evolution is characterized by the AE waveform with a long duration of over 0.15 ms and a power spectrum with a relatively narrow frequency distribution of around 0.6 MHz and the maximum amplitude at about 0.1 MHz.

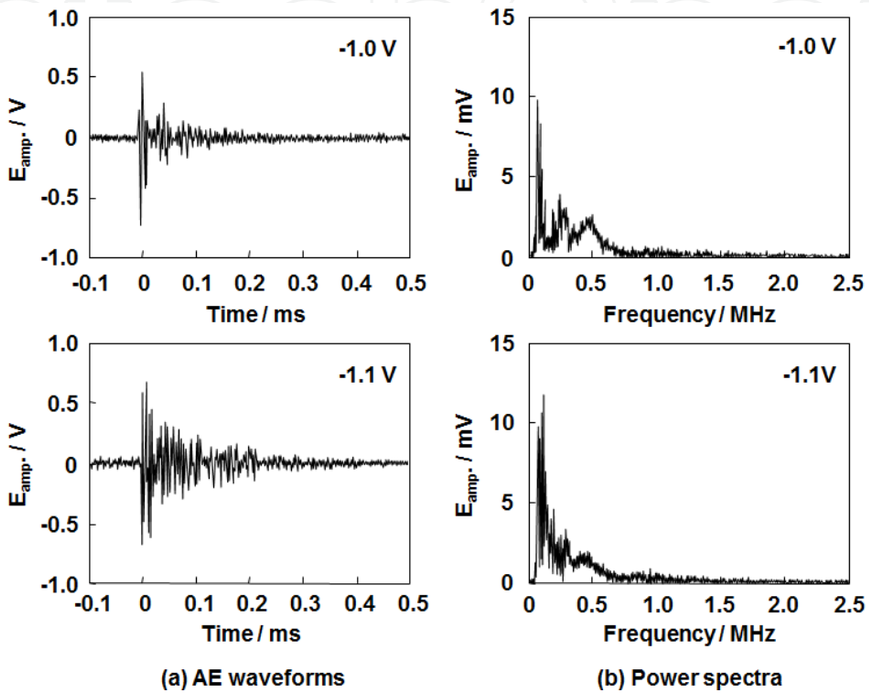

Fig. 3. (a) AE waveforms and (b) power spectra for hydrogen evolution on a Cu electrode at -1.0 and -1.1 V vs. Hg/HgO in a 6 M KOH aqueous solution. (Reprinted with permission from *Electrochem. Solid-State Lett.*, 9, A504 (2006). Copyright 2006 The Electrochemical Society.)

4. Acoustic emission from hydrogen storage alloy negative electrodes while charging

4.1 $MmNi_{3.6}Mn_{0.4}Al_{0.3}Co_{0.7}$ electrode

AE waveforms and power spectra for a $MmNi_{3.6}Mn_{0.4}Al_{0.3}Co_{0.7}$ (106-125 μm) negative electrode were measured every 1 h during the 1st charging process and summarized in Fig. 4. AE waveforms and power spectra observed for the initial 1 h were quite different from those identified as the hydrogen evolution. In the former, AE waveforms have a sharp spike with duration shorter than 0.1 ms and larger amplitude, and power spectra have wide frequency distribution, particularly some peaks at frequencies more than 0.6 MHz, which is not characteristic of hydrogen evolution. The AE waveforms and power spectra, however, changed to those due to hydrogen evolution between 1 h and 2 h after start of the charging process. During the first half of the 1st charging process, a phenomenon other than hydrogen evolution, probably cracking of individual alloy particles, must have occurred. From the comparison of scanning electron micrographs (see Fig. 7) for the surface of

$MmNi_{3.6}Mn_{0.4}Al_{0.3}Co_{0.7}$ particles before and after the 1st charge-discharge cycle, a number of large and small cracks were observed on the alloy surface after the charge-discharge cycle. Therefore, it is inferred that the alloy particles cracked in the first half of the charging process. Thus the cracking of alloy particles is characterized by a burst-type AE waveform with duration shorter than 0.1 ms and large amplitude, and a power spectrum with wide frequency distribution, particularly with some peaks at frequencies more than 0.6 MHz.

In the 2nd charging process, AE waveforms and power spectra for the $MmNi_{3.6}Mn_{0.4}Al_{0.3}Co_{0.7}$ electrode measured every 1 h are summarized in Fig. 5. The AE waveforms after 1 h and 2 h had a sharp spike with duration shorter than 0.1 ms, but their amplitude was much smaller than that in the 1st charging process. In addition, power spectra after 1 h and 2h had wide frequency distribution. These results clearly exhibit that the cracking of alloy particles occurs at 1 h and 2 h after start of the 2nd charging process. On the other hand, the AE waveforms and power spectra at the beginning and 3 h suggested hydrogen evolution. Thus, in the 2nd charging process the cracking occurred preferentially after 1 h and 2 h after start of charging while hydrogen evolution proceeded throughout charging, but it was not vigorous compared to the 1st charging process.

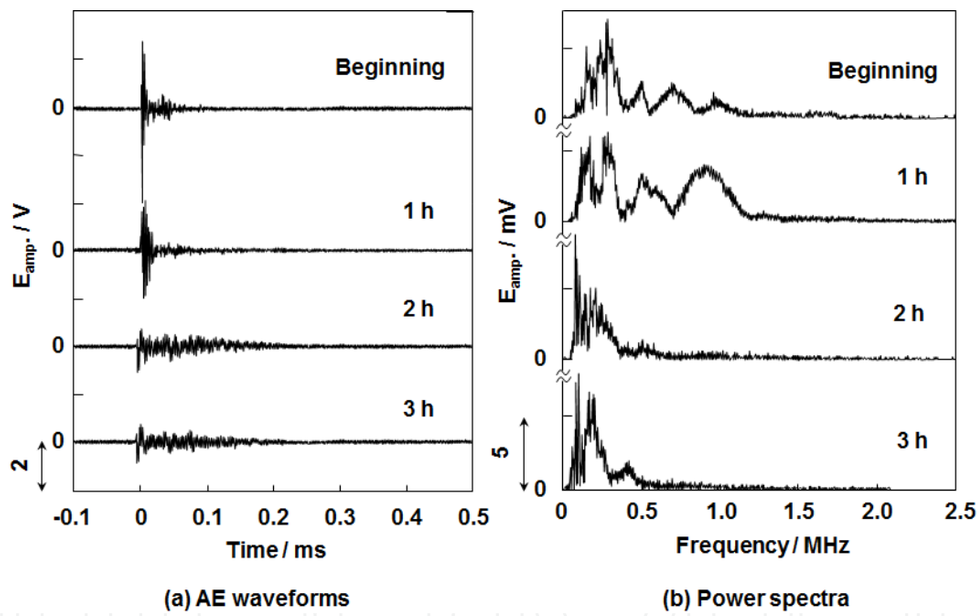

Fig. 4. (a) AE waveforms and (b) power spectra for electrochemical phenomena on a $MmNi_{3.6}Mn_{0.4}Al_{0.3}Co_{0.7}$ (106-125 μm) negative electrode measured every 1 h during the 1st charging process. (Reprinted with permission from *Electrochem. Solid-State Lett.*, 9, A504 (2006). Copyright 2006 The Electrochemical Society.)

Figure 6 shows initial activation behavior for a $MmNi_{3.6}Mn_{0.4}Al_{0.3}Co_{0.7}$ electrode and time history of frequency of AE signals and time course of electrode potential in the 1st, 2nd or 6th charging process. In each time history, the frequency of AE signals is defined as the number of AE signals with amplitude over a threshold of 0.5 V for one minute. In the initial activation behavior, discharge capacity was ca. 140 mAh $g(alloy)^{-1}$ at 1st cycle, and then it increased with cycle number and approximately reached a constant value (ca. 220 mAh $g(alloy)^{-1}$) at the 4th cycle, indicating that the initial activation was completed for four charge-discharge cycles.

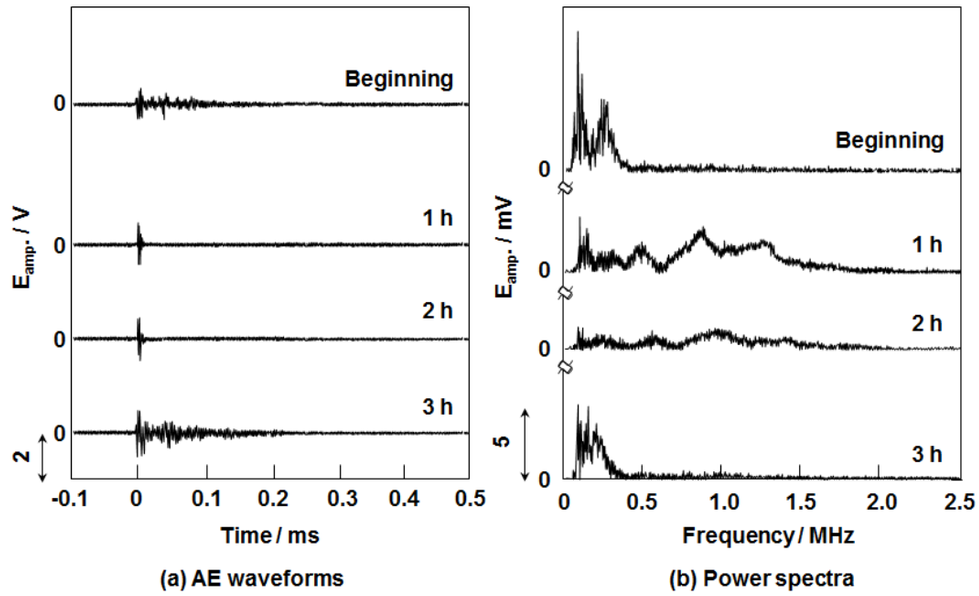

Fig. 5. (a) AE waveforms and (b) power spectra for electrochemical phenomena on a $MmNi_{3.6}Mn_{0.4}Al_{0.3}Co_{0.7}$ (106-125 μm) negative electrode measured every 1 h during the 2nd charging process. (Reprinted with permission from *J. Alloys Compd.*, 446-447, 681 (2007). Copyright 2007 Elsevier.)

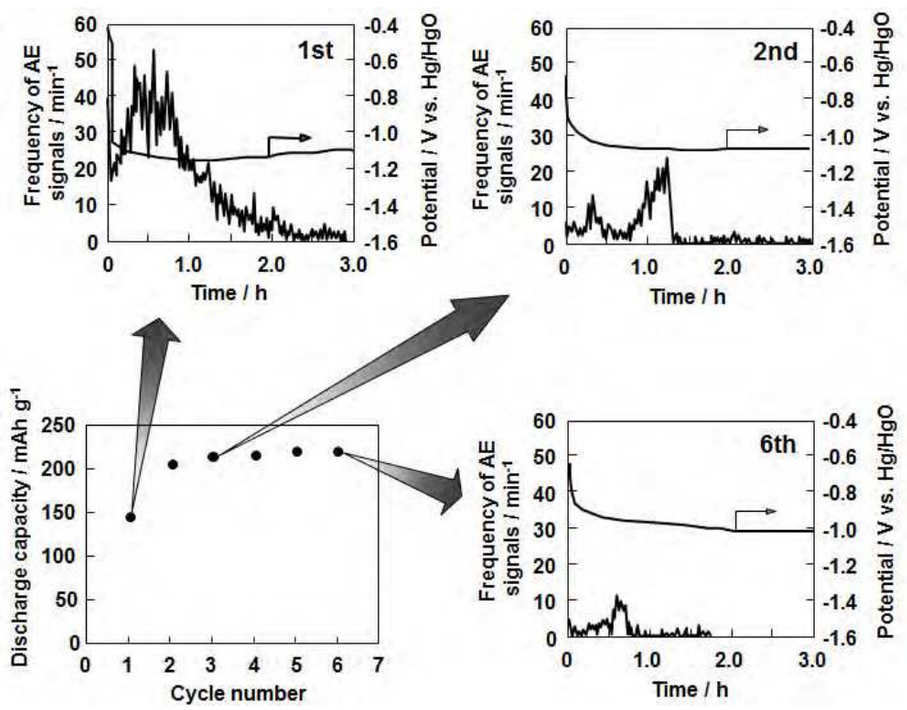

Fig. 6. Initial activation behavior for a $MmNi_{3.6}Mn_{0.4}Al_{0.3}Co_{0.7}$ (106-125 μm) negative electrode and its time history of frequency of AE signals and electrode potential in 1st, 2nd and 6th charging processes. (Reprinted with permission from *J. Alloys Compd.*, 446-447, 681 (2007). Copyright 2007 Elsevier.)

In the first half of the 1st charging process, a large number of AE signals were observed. This comes from the cracking based on lattice expansion due to hydrogen absorption, which has also been confirmed by the AE wave forms and power spectra in the same period (Fig. 4). The electrode potential reached ca. -1.1 V immediately after start of charging and then it hardly changed during the charging. This suggests that hydrogen evolution proceeds throughout the charging. Figure 7 shows scanning electron micrographs of the $MmNi_{3.6}Mn_{0.4}Al_{0.3}Co_{0.7}$ electrode surface before charging and after the 1st, 2nd and 6th cycles. As described above, a number of large and small cracks appeared on the alloy surface after the 1st charge-discharge cycle, supporting a large number of AE signals observed in Fig. 6. In the 2nd charging process, the frequency of AE signals greatly decreased compared to the 1st charging process as shown in Fig. 6, and the scanning electron micrograph after 2nd charging showed that smaller cracks increased compared to after 1st charging. These results indicate that the fine cracking of alloy particles occur in the 2nd charging process. After 6th cycle, the number of AE signals significantly decreased and discharge capacity showed a constant value as shown in Fig. 6. A lot of finer cracks were observed after 6th cycle as shown in Fig. 7. Thus, *in situ* analysis by the AE technique confirms the well-known conclusion that during initial activation the $MmNi_{3.6}Mn_{0.4}Al_{0.3}Co_{0.7}$ particles frequently cracks and the increase in the cracks with cycle number leads to the increase in discharge capacity.

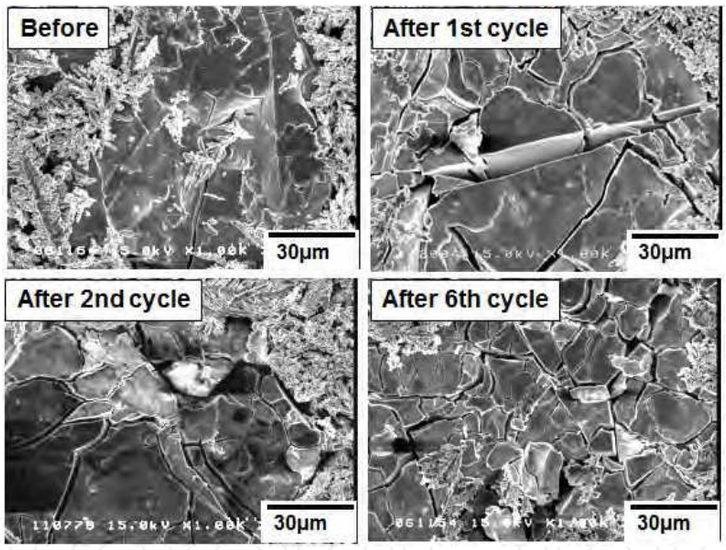

Fig. 7. Scanning electron micrographs of a $MmNi_{3.6}Mn_{0.4}Al_{0.3}Co_{0.7}$ (106-125 μm) negative electrode surface before charging and after 1st, 2nd and 6th charging processes. (Reprinted with permission from *J. Alloys Compd.*, 446-447, 681 (2007). Copyright 2007 Elsevier.)

The pattern of cracking during charging may change with size of alloy particles. The cracking behavior of small alloy particles was also characterized by the AE technique. Figure 8 shows initial activation behavior for a $MmNi_{3.6}Mn_{0.4}Al_{0.3}Co_{0.7}$ (less than 25 μm) electrode and time history of frequency of AE signals and time course of electrode potential in the 1st, 2nd or 6th charging process. In this case, discharge capacity was ca. 220 mAh $g(alloy)^{-1}$ even at the 1st cycle, and then it was almost constant. This indicates that the small alloy particles do not have to be activated. In the time history at the 1st cycle, there were very few AE signals compared to the time history for the larger alloy particles (see Fig. 6), suggesting that the cracking of the small alloy particles poorly occurred probably because the lattice stress of the small particles

with lattice expansion was not so large as larger particles. The similar results were observed in the 2nd and 6th cycles. Figure 9 shows scanning electron micrographs of the $MmNi_{3.6}Mn_{0.4}Al_{0.3}Co_{0.7}$ (less than 25 μm) electrode surface before charging and after 1st, 2nd and 6th cycles. There were very few cracks even after the 1st cycle, which proves poor cracking of the small ally particles. Thus the small particles with sizes of less than 25 μm are hard to crack even though they absorb a great amount of hydrogen in charging.

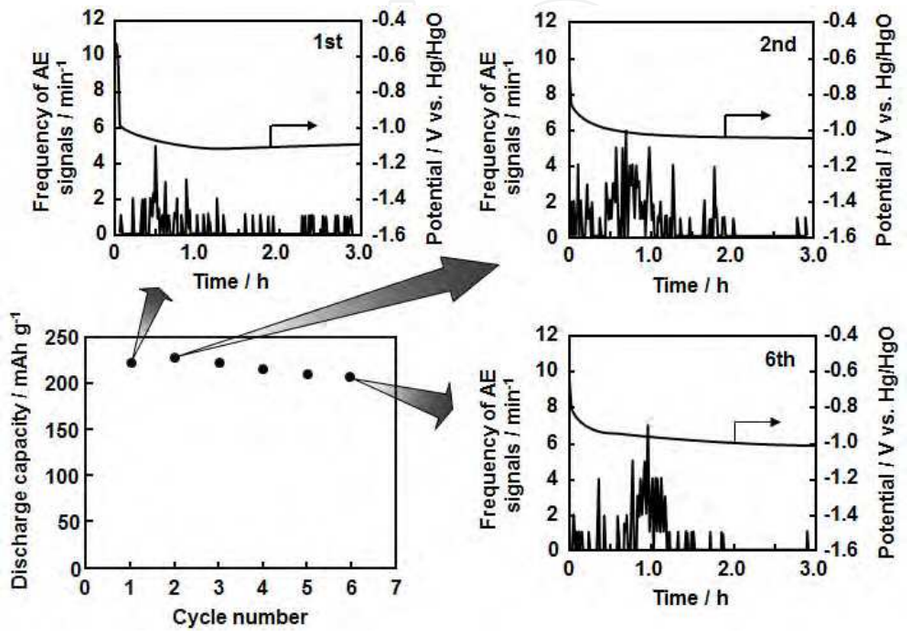

Fig. 8. Initial activation behavior for a $MmNi_{3.6}Mn_{0.4}Al_{0.3}Co_{0.7}$ (less than 25 μm) electrode and time history of frequency of AE signals and time course of electrode potential in the 1st, 2nd or 6th charging process.

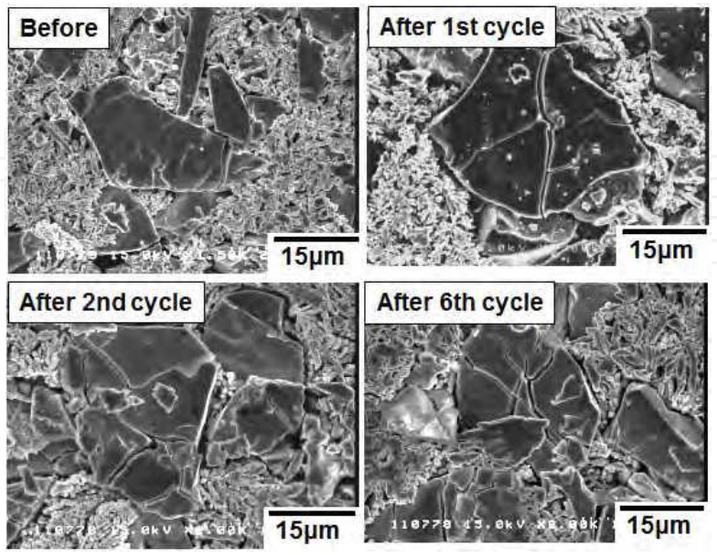

Fig. 9. Scanning electron micrographs of a $MmNi_{3.6}Mn_{0.4}Al_{0.3}Co_{0.7}$ (less than 25 μm) negative electrode surface before charging and after 1st, 2nd and 6th charging processes.

Figure 10 shows AE waveforms and power spectra for the $MmNi_{3.6}Mn_{0.4}Al_{0.3}Co_{0.7}$ (less than 25 μm) negative electrode measured every 1 h during the 1st charging process. AE waveforms and power spectra at 1 h after start of charging suggested the cracking of particles, but otherwise hydrogen evolution was dominant. Moreover, in the 1st charging process electrode potential reached ca. -1.1 V immediately after start of charging and then it hardly changed during the charging (Fig. 8), suggesting that hydrogen evolution proceeded throughout the charging.

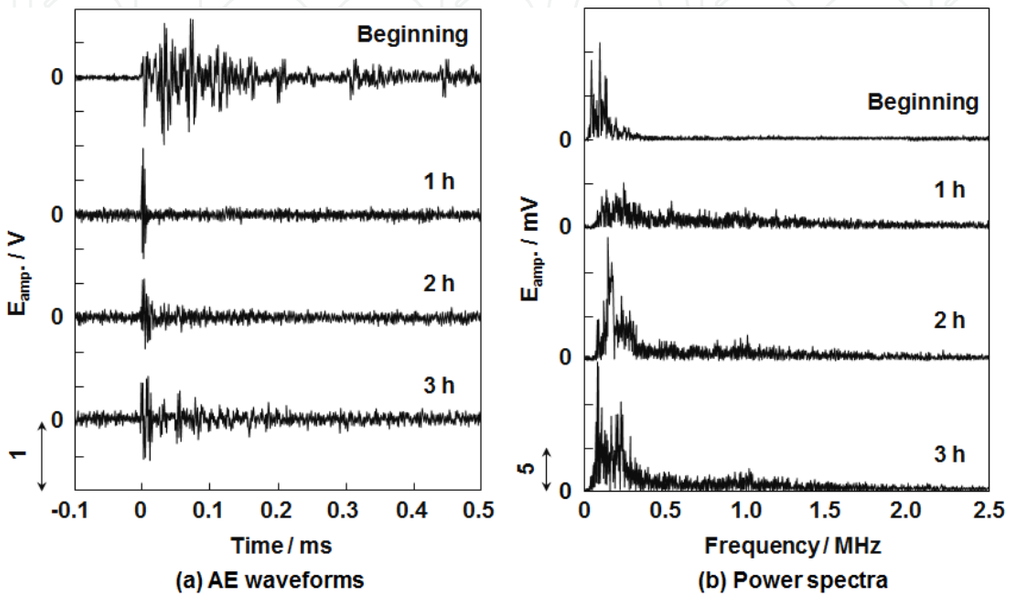

Fig. 10. (a) AE waveforms and (b) power spectra for electrochemical phenomena on a $MmNi_{3.6}Mn_{0.4}Al_{0.3}Co_{0.7}$ (less than 25 μm) negative electrode measured every 1 h during the 1st charging process.

4.2 $TiV_{1.8}Cr_{0.3}Ni_{0.3}$ electrode

V-based hydrogen storage alloys with a body-centered cubic (BCC) structure as a main phase are potential negative electrode active materials for nickel-metal hydride batteries and hydrogen reservoirs for fuel cells because of high hydrogen storage capacity per volume. A $TiV_{2.1}Ni_{0.3}$ negative electrode, one of V-based alloys prepared by the Author's laboratory, had high discharge capacity of 460 mAh g^{-1} and poor cycle durability. To improve cycle durability, it is effective to substitute Cr for the V constituent of $TiV_{2.1}Ni_{0.3}$ because the oxidative dissolution of V into an electrolyte solution is suppressed. In the preliminary experiments, a $TiV_{1.8}Cr_{0.3}Ni_{0.3}$ electrode significantly improved cycle durability. So the charging behavior of the $TiCr_{0.3}V_{1.8}Ni_{0.3}$ electrode was analyzed by the AE technique.

Time history of frequency of AE signals and electrode potential in the 1st, 2nd and 6th charging processes and initial activation behavior for the $TiV_{1.8}Cr_{0.3}Ni_{0.3}$ (75-106 μm) electrode were summarized in Fig. 11. In the 1st charging process, a large number of AE signals were observed for initial 2 h. Since electrode potential was ca. -1.1 V in this term, hydrogen evolution is also expected to proceed.

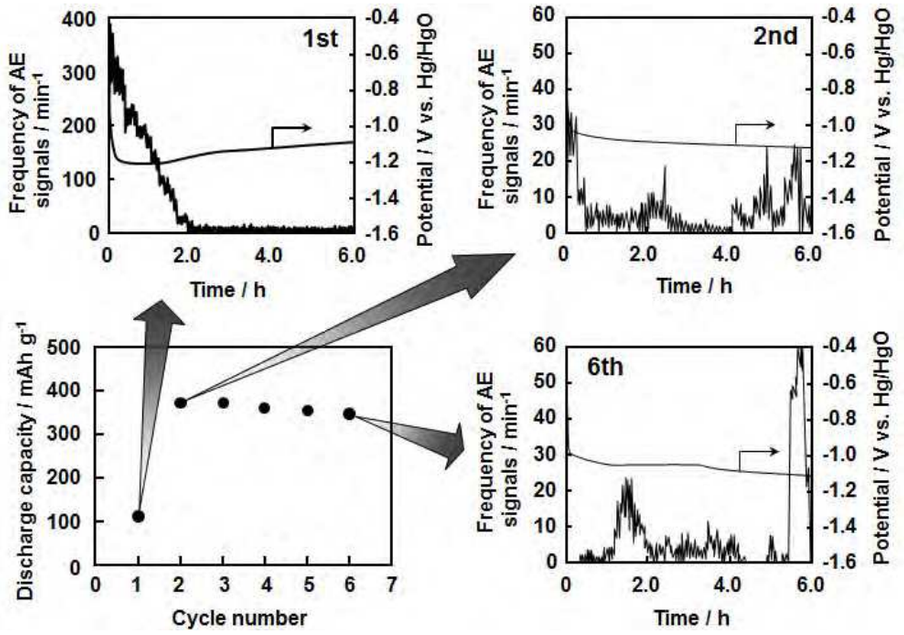

Fig. 11. Initial activation behavior for a $TiV_{1.8}Cr_{0.3}Ni_{0.3}$ (75-106 μm) electrode and time history of frequency of AE signals and time course of electrode potential in the 1st, 2nd or 6th charging process. (Reprinted with permission from *J. Alloys Compd.*, 446-447, 681 (2007). Copyright 2007 Elsevier.)

Figure 12 and Fig. 13 show AE waveforms and power spectra for the $TiV_{1.8}Cr_{0.3}Ni_{0.3}$ (75-106 μm) electrode measured every 1 h during the 1st charging process. Both the AE waveform and power spectrum at 1 h exhibit that hydrogen evolution proceeds, supporting the inference from Fig. 11. In further charging, the AE waveform and power spectrum due to

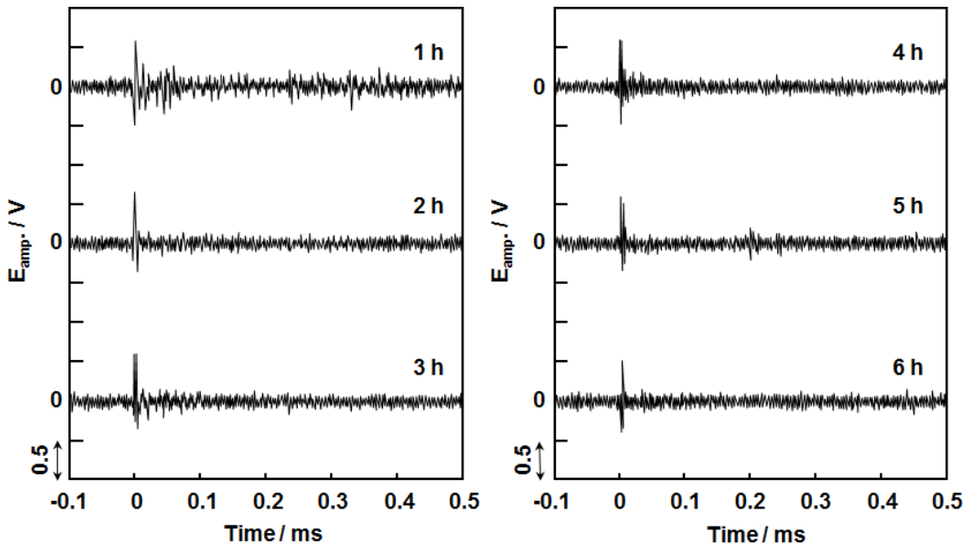

Fig. 12. AE waveforms for electrochemical phenomena on a $TiV_{1.8}Cr_{0.3}Ni_{0.3}$ (75-106 μm) negative electrode measured every 1 h during the 1st charging process. (Reprinted with permission from *J. Alloys Compd.*, 446-447, 681 (2007). Copyright 2007 Elsevier.)

the cracking were mainly observed, but judging from the time history of the frequency of AE signals, the cracking was sporadic. The $TiV_{1.8}Cr_{0.3}Ni_{0.3}$ electrode began to crack later than the $MmNi_{3.6}Mn_{0.4}Al_{0.3}Co_{0.7}$ electrode, suggesting that the former was more patient for cracking than the latter. The maximum amplitude of AE waveforms was just ca. one forth of that for the $MmNi_{3.6}Mn_{0.4}Al_{0.3}Co_{0.7}$ electrode, suggesting that relatively small cracks were formed on the $TiV_{1.8}Cr_{0.3}Ni_{0.3}$ alloy surface. Figure 14 shows scanning electron micrographs of the $TiV_{1.8}Cr_{0.3}Ni_{0.3}$ (75-106 μm) electrode surface before charging and after the 1st, 2nd and 6th cycles. The scanning electron micrograph after 1st cycle exhibits that a few and relatively small cracks were observed on the $TiV_{1.8}Cr_{0.3}Ni_{0.3}$ particles, which agreed with the suggestion from the AE measurements.

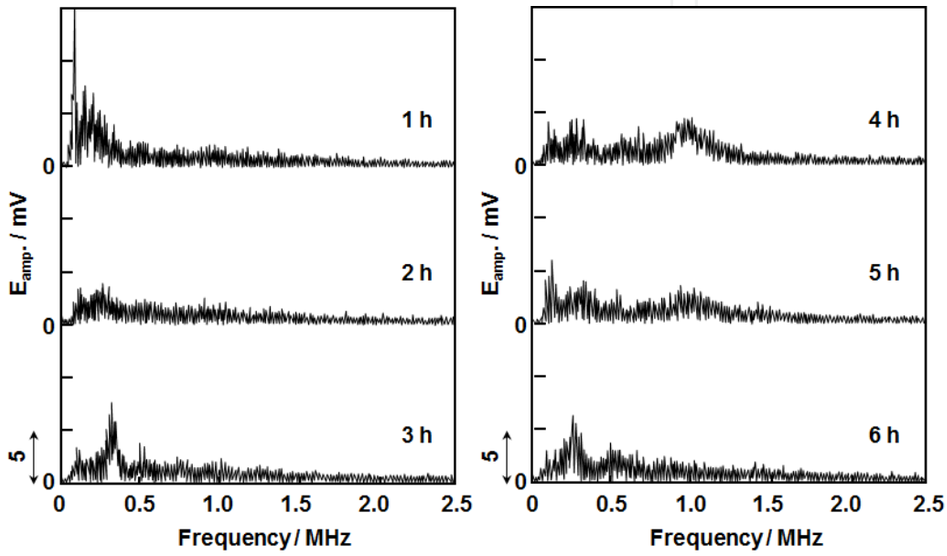

Fig. 13. Power spectra for electrochemical phenomena on a $TiV_{1.8}Cr_{0.3}Ni_{0.3}$ (75-106 μm) negative electrode measured every 1 h during the 1st charging process. (Reprinted with permission from *J. Alloys Compd.*, 446-447, 681 (2007). Copyright 2007 Elsevier.)

In Fig. 11, frequency of AE signals decreased greatly with repeating charge-discharge cycles. The AE waveforms (Fig. 15) and power spectra (Fig. 16) in the 2nd charging process showed that the cracking based on hydrogen absorption occurred from the beginning. As can be seen from charge-discharge cycle performance in Fig. 11, discharge capacity greatly increases for the first 2 cycles due to initial activation. In the initial activation the surface oxides inhibiting hydrogen absorption into alloy seemed to be removed by sporadic cracking of alloy particles during the 1st cycle to expose fresh surface, leading to hydrogen absorption from the beginning of the 2nd charging and the increase in discharge capacity. Moreover, Fig. 14 shows that the $TiV_{1.8}Cr_{0.3}Ni_{0.3}$ particles are not frequently pulverized like the $MmNi_{3.6}Mn_{0.4}Al_{0.3}Co_{0.7}$ particles in initial activation. Nevertheless the former has higher discharge capacity than the latter and is comparable to the $TiV_{2.1}Ni_{0.3}$ electrode. The $TiV_{1.8}Cr_{0.3}Ni_{0.3}$ is also composed of two phases like $TiV_{2.1}Ni_{0.3}$. The main phase has a Ti-V solid solution BCC structure and serves as the main hydrogen reservoir. On the other hand, the secondary phase has a TiNi-type structure and serves as a catalyst for generating hydrogen atoms and transferring them into the main phase. The partial substitution with

the Cr component effectively inhibits corrosion and does not bring any serious problems on hydrogen diffusion in alloy and electron transfer at electrode surface.

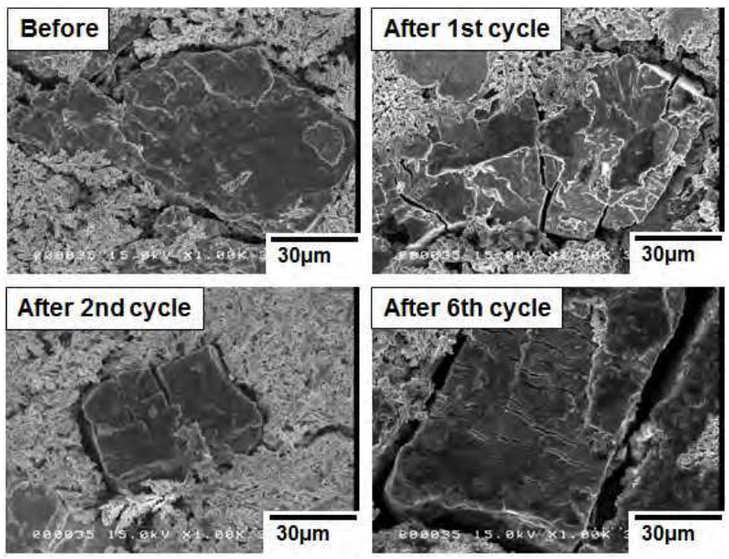

Fig. 14. Scanning electron micrographs of a $TiV_{1.8}Cr_{0.3}Ni_{0.3}$ (75-106 μm) negative electrode surface before charging and after 1st, 2nd and 6th charging processes. (Reprinted with permission from *J. Alloys Compd.*, 446-447, 681 (2007). Copyright 2007 Elsevier.)

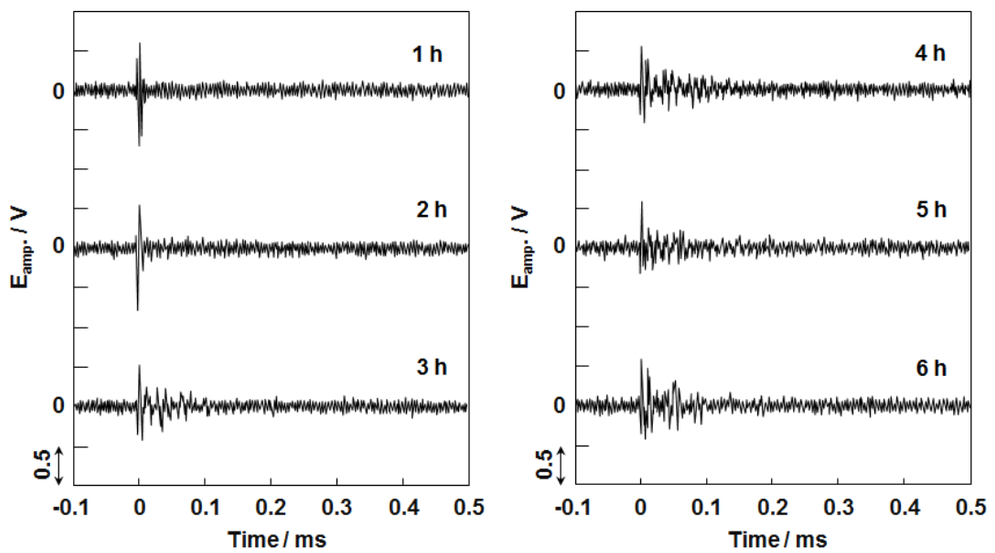

Fig. 15. AE waveforms for electrochemical phenomena on a $TiV_{1.8}Cr_{0.3}Ni_{0.3}$ (75-106 μm) negative electrode measured every 1 h during the 2nd charging process.

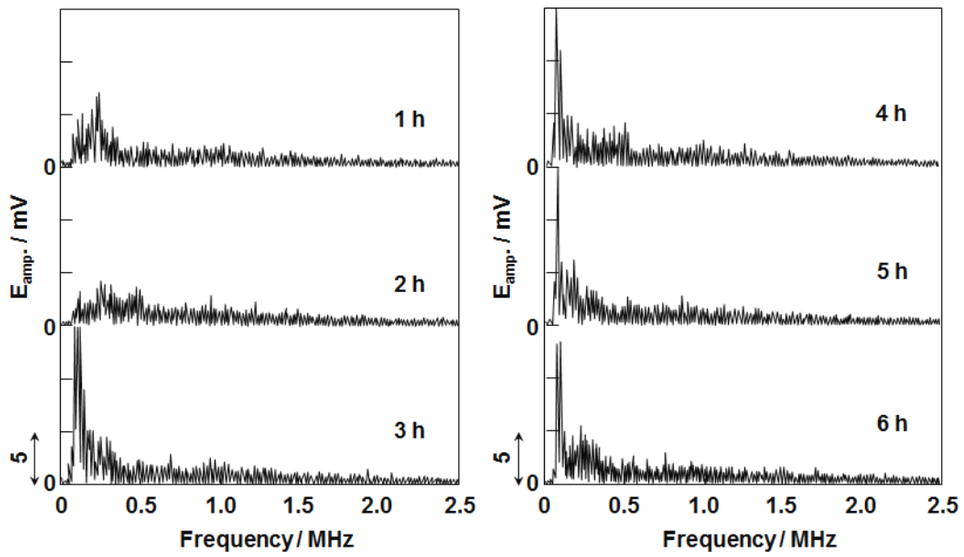

Fig. 16. Power spectra for electrochemical phenomena on a $TiV_{1.8}Cr_{0.3}Ni_{0.3}$ (75-106 μm) negative electrode measured every 1 h during the 2nd charging process.

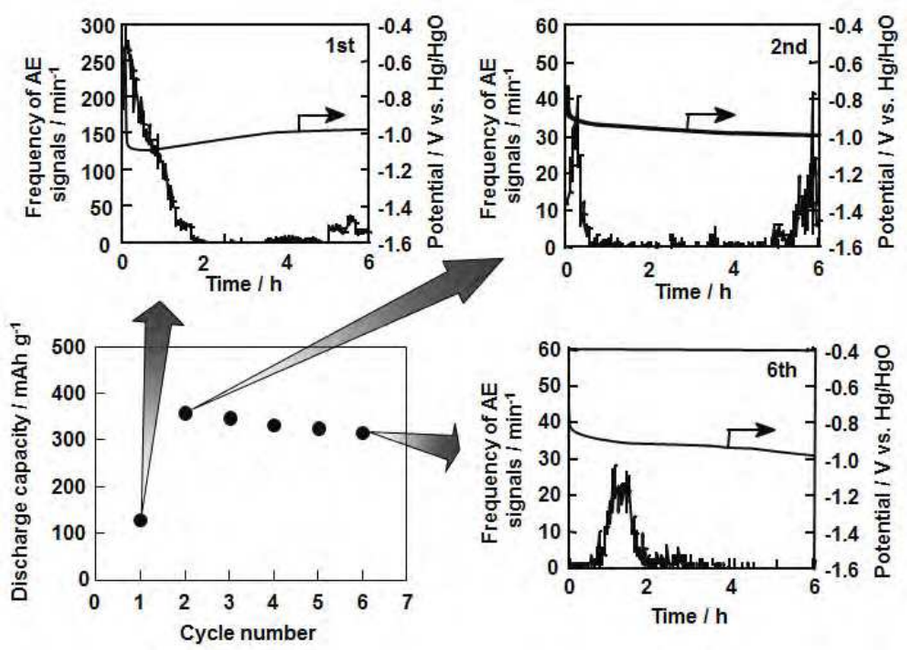

Fig. 17. Initial activation behavior for a $TiV_{1.8}Cr_{0.3}Ni_{0.3}$ (25-53 μm) electrode and time history of frequency of AE signals and time course of electrode potential in the 1st, 2nd or 6th charging process.

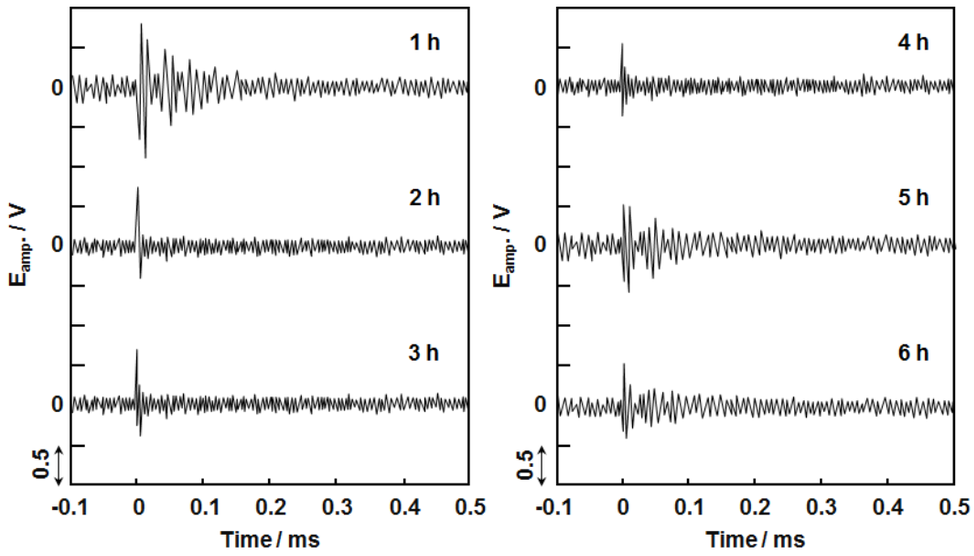

Fig. 18. AE waveforms for electrochemical phenomena on a $TiV_{1.8}Cr_{0.3}Ni_{0.3}$ (25-53 μm) negative electrode measured every 1 h during the 1st charging process.

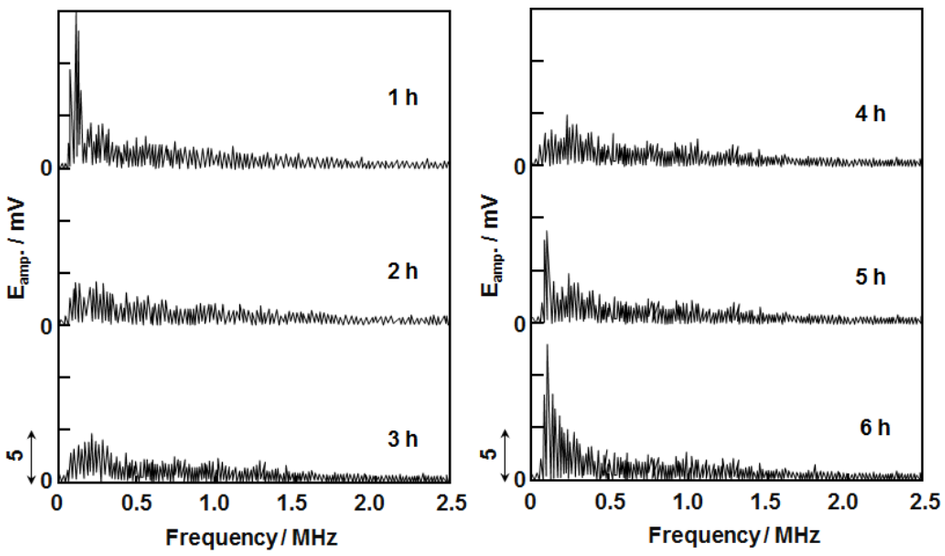

Fig. 19. Power spectra for electrochemical phenomena on a $TiV_{1.8}Cr_{0.3}Ni_{0.3}$ (25-53 μm) negative electrode measured every 1 h during the 1st charging process.

Figure 17 shows initial activation behavior for a $TiV_{1.8}Cr_{0.3}Ni_{0.3}$ (25-53 μm) electrode and time history of frequency of AE signals and time course of electrode potential in the 1st, 2nd or 6th charging process. From Fig. 11 and Fig. 17, charge-discharge cycle performance is independent of particle size of the alloy. As for time history, in the 1st charging process, a large number of AE signals were observed for initial 2 h, which is similar to the alloy particles with sizes of 75-106 μm. The frequency of AE signals significantly decreased with repeating charge-discharge cycling. Electrode potential in this term, however, was -1.0 V which was more positive compared to the $TiV_{1.8}Cr_{0.3}Ni_{0.3}$ (75-106 μm) electrode. In this case hydrogen evolution is expected to proceed but it seems to be poor. This is also suggested from Fig. 18 and Fig. 19. Both AE waveforms and power spectra in the 1st charging process show hydrogen evolution occurs for initial 2 h, and then cracking also occurs. But the term for cracking was shorter than that for the $TiV_{1.8}Cr_{0.3}Ni_{0.3}$ (75-106 μm) electrode, suggesting that the cracking was poorer for smaller alloy particles. Figure 20 shows scanning electron micrographs of the $TiV_{1.8}Cr_{0.3}Ni_{0.3}$ (25-53 μm) electrode surface before charging and after the 1st, 2nd and 6th cycles. The scanning electron micrograph after 1st cycle exhibits that very few cracks were observed on the $TiV_{1.8}Cr_{0.3}Ni_{0.3}$ particles, indicating that the number of cracks decreased with particle size. The number of cracks slightly increased with cycle number.

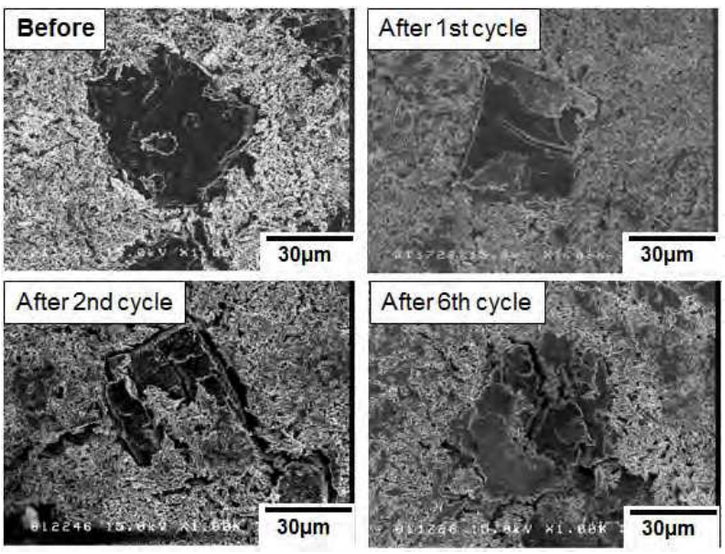

Fig. 20. Scanning electron micrographs of a $TiV_{1.8}Cr_{0.3}Ni_{0.3}$ (25-53 μm) negative electrode surface before charging and after 1st, 2nd and 6th charging processes.

5. Conclusion

In charging of hydrogen storage alloy negative electrodes, $MmNi_{3.6}Mn_{0.4}Al_{0.3}Co_{0.7}$ and $TiV_{1.8}Cr_{0.3}Ni_{0.3}$ electrodes, cracking based on hydrogen absorption into alloy and hydrogen evolution were clearly discriminated using an AE technique in terms of waveforms, power spectra and time history of the AE signals. The $MmNi_{3.6}Mn_{0.4}Al_{0.3}Co_{0.7}$ (106-125 μm) particles cracked intensively in the first half of the 1st charging process and were broken down with many large and small cracks during initial activation. In contrast, the $MmNi_{3.6}Mn_{0.4}Al_{0.3}Co_{0.7}$ particles (less than 25 μm) had high discharge capacity even in the 1st charging process, but it poorly cracked, suggesting that the particle size was enough small to diffuse throughout the particles without cracking. As for the $TiCr_{0.3}V_{1.8}Ni_{0.3}$ particles, irrespective of particle size the cracking sporadically occurred after hydrogen evolution in the 1st charging process and the AE signals for the cracking were very weak compared to those for the $MmNi_{3.6}Mn_{0.4}Al_{0.3}Co_{0.7}$ particles, indicating that the $TiCr_{0.3}V_{1.8}Ni_{0.3}$ particles were hard to crack. Moreover, the smaller particles (25-53 μm) were more resistant to cracking than the larger ones (75-106 μm).

Lithium ion battery (LIB) is the primary candidate for plug-in hybrid electric vehicles and electric vehicles because of their high energy and power density compared to Ni-MH battery. At both electrodes in LIB, lithium intercalation/deintercalation reactions occur. Recently, to improve energy and power density more and more, researches on new negative electrode active materials with high capacity like Si, Sn etc. have been actively performed. Such active material particles are easy to crack with repeated lithium intercalation/deintercalation, leading to capacity loss in a LIB or short lifetime. So the *in situ* real analysis of stress and cracking are important for clarifying the mechanism of capacity degradation, and the electrochemical AE technique must be a powerful tool.

6. References

Bernard, J.; Boinet, M.; Chatenet, M. & Dalard, F. (2005). Contribution of the Acoustic Emission Technique to Study Aluminum Behavior in Aqueous Alkaline Solution. *Electrochem. Solid-State Lett.*, Vol. 8, No. 7, (July 2005), pp. E53-E55, ISSN 0013-4651

Darowicki, K.; Orlikowski, J.; Arutunow, A. & Jurczak, W. (2005). Passive Layer Cracking Studies Performed on A95056 Aluminum Alloy by DEIS and Acoustic Emission. *Electrochem. Solid-State Lett.*, Vol. 8, No. 8, (August 2005), pp. B55-B57, ISSN 0013-4651

Etiemble, A.; Idrissi, H. & Roue, L. (2011). On the Decrepitation Mechanism of MgNi and $LaNi_5$-Based Electrodes Studied by in Situ Acoustic Emission. *J. Power Sources*, Vol. 196, No. 11, (June 2011), pp. 5168-5173, ISSN 0378-7753

Fregonese, M.; Idrissi, H.; Mazille, H.; Renaud, L. & Cetre, Y. (2001). Initiation and Propagation Steps in Pitting Corrosion of Austenitic Stainless Steels: Monitoring by Acoustic Emission. *Corrosion Science*, Vol. 43, No. 4, (April 2001), pp. 627-641, ISSN 0010-928X

Inoue, H.; Miyauchi, R.; Shin-ya, R.; Choi, W. –K. & Iwakura, C. (2002). Charge–Discharge Characteristics of $TiV_{2.1}Ni_{0.3}$ Alloy Surface-Modified by Ball-Milling with Ni or Raney Ni. *J. Alloys Compd.*, Vol. 330-332 (January 2002) pp. 597-600, ISSN 0925-8388

Inoue, H.; Tsuzuki, R.; Nohara, S. & Iwakura, C. (2006). *In Situ* Monitoring of Hydrogen Storage Alloy Negative Electrode during Charging by an Acoustic Emission Technique. *Electrochem. Solid-State Lett.*, Vol. 9, No. 11, (November 2006), pp. A504-A506, ISSN 0013-4651

Inoue, H.; Tsuzuki, R.; Nohara, S. & Iwakura, C. (2007). Characterization of Initial Activation Behavior for Hydrogen Storage Alloys by Acoustic Emission Technique. *J. Alloys Compd.*, Vol. 446-447, (October 2007), pp. 681-686, ISSN 0925-8388

Iwakura, C.; Choi, W. –K.; Miyauchi, R. & Inoue, H. (2000). Electrochemical and Structural Characterization of Ti-V-Ni Hydrogen Storage Alloys with BCC Structure. *J. Electrochem. Soc.*, Vol. 147, No. 7, (July 2000). pp. 2503-2506, ISSN 0013-4651

Iwakura, C.; Inoue, H. & Nohara, S. (2001). Hydrogen–Metal Systems: Electrochemical Reactions (Fundamentals and Applications), In: *Encyclopedia of Materials: Science and Technology*, Buschow, K.H.J.; Cahn, R.; Flemings M.; Ilschner B.; Kramer E.; Mahajan S. & Veyssiere, P., pp. 3929-3941, Elsevier Science, ISBN 10**:** 0-08-043152-6, Amsterdam

Kalisvaart, W. P.; Latroche, M.; Cuevas, F. & Notten, P. H. L. (2008). In Situ Neutron Diffraction Study on Pd-doped $Mg_{0.65}Sc_{0.35}$ Electrode Material. *J. Solid State Chem.*, Vol. 181, No. 5, (May 2008), pp. 1141-1148, ISSN 0022-4596

Kalnaus, S., Rhodes, K. & Daniel, C. (2011). A Study of Lithium Ion Intercalation Induced Fracture of Silicon Particles Used as Anode Material in Li-ion Battery. *J. Power Sources*, Vol. 196, No. 19, (October 2011), pp. 8116-8124, ISSN 0378-7753

Kuriyama, N.; Chartouni, D.; Tsukahara, M.; Takahashi, K.; Takeshita, H. T.; Tanaka, H.; Schlapbach, L.; Sakai, T. & Uehara, I. (1998). Scanning Tunnelling Microscopy In Situ Observation of Phase-Selective Cathodic Hydrogenation of a V-Ti-Ni-Based Multiphase Alloy Electrode. *Electrochem. Solid-State Lett.*, Vol. 1, No. 1, (January 1998), pp. 37-38, ISSN 0013-4651

Notten, P. H. L.; Daams, J. L. C. & Einerhand, R. E. F. (1994). On the Nature of the Electrochemical Cycling of Non-stoichiometric $LaNi_5$-based Hydride-forming Compounds Part II. In Situ X-ray Diffractiometry. *J. Alloys Compd.*, Vol. 210, No. 1-2, (August 1994), pp. 233-241, ISSN 0925-8388

Ohzuku, T.; Tomura, H. & Sawai, K. (1997). Monitoring of Particle Fracture by Acoustic Emission during Charge and Discharge of Li/MnO_2 Cells. *J. Electrochem. Soc.*, Vol. 144, No. 10, (October 1997), pp. 3496-3500, ISSN 0013-4651

Ramesh, R.; Mukhopadhyay, C. K.; Jayakumar, T. & Raj, B. (1998). Characterization of Acoustic Emission generated during Electrochemical Charging and Discharging of Hydrogen in Palladium. *Scr. Met.*, Vol. 38, No. 4, (January 1998), pp. 661-665, ISSN 1359-6462

Rhodes, K.; Dudney, N.; Lara-Curzio, E. & Daniel, C. (2010). Understanding the Degradation of Silicon Electrodes for Lithium-Ion Batteries Using Acoustic Emission. *J. Electrochem. Soc.*, Vol. 157, No. 12, (December 2010), pp. A1354-A1360, ISSN 0013-4651

Sawai, K.; Tomura,H. & Ohzuku T. (1998). Acoustic Emission Histometry for Battery Material Research. *Denki Kagaku*, Vol. 66, No. 3, (March 1998), pp. 301-307, ISSN 1344-3542

Tsai, S. T. & Shih,H. C. (1998). Correlation Between Acoustic Emission Signals and Hydrogen Permeation in High Strength, Low Alloy Steel Cracking in Wet H_2S. *J. Electrochem. Soc.*, Vol. 145, No. 6, (June 1998), pp. 1968-1976, ISSN 0013-4651

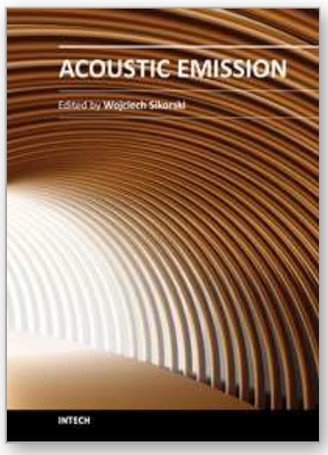

Acoustic Emission

Edited by Dr. Wojciech Sikorski

ISBN 978-953-51-0056-0
Hard cover, 398 pages
Publisher InTech
Published online 02, March, 2012
Published in print edition March, 2012

Acoustic emission (AE) is one of the most important non-destructive testing (NDT) methods for materials, constructions and machines. Acoustic emission is defined as the transient elastic energy that is spontaneously released when materials undergo deformation, fracture, or both. This interdisciplinary book consists of 17 chapters, which widely discuss the most important applications of AE method as machinery and civil structures condition assessment, fatigue and fracture materials research, detection of material defects and deformations, diagnostics of cutting tools and machine cutting process, monitoring of stress and ageing in materials, research, chemical reactions and phase transitions research, and earthquake prediction.

InTech Europe
University Campus STeP Ri
Slavka Krautzeka 83/A
51000 Rijeka, Croatia
Phone: +385 (51) 770 447
Fax: +385 (51) 686 166
www.intechopen.com

InTech China
Unit 405, Office Block, Hotel Equatorial Shanghai
No.65, Yan An Road (West), Shanghai, 200040, China
中国上海市延安西路65号上海国际贵都大饭店办公楼405单元
Phone: +86-21-62489820
Fax: +86-21-62489821

IntechOpen